TECTONICS

Supporting Information for "Magmatism, migrating topography, and the onset of faulting in the northern Basin and Range province, western USA"

Jens-Erik Lund Snee[1] and Elizabeth L. Miller[2]

[1]Department of Geophysics, Stanford University, 397 Panama Mall, Mitchell Bld. 3rd Floor, Stanford, CA 94305
[2]Department of Geological Sciences, Stanford University, 450 Serra Mall Bld. 320, Room 118, Stanford, CA 94305

Contents of this file

Additional Supporting Information (Files uploaded separately)

Introduction

This supplement contains appendices that provide descriptions of methods for U-Pb detrital zircon geochronology and stable isotope analyses, a figure with probability density plots for ages obtained from the detrital zircon analyses, an appendix with explanation of techniques used for establishing depositional thicknesses and ages, a summary of relevant prior work and controversies related to the Great Basin region, a figure providing references for the ages of Great Basin paleodrainages, and data tables reporting the results of those analyses.

Text S1. Methods for U-Pb Detrital Zircon Geochronologic Analyses

We sampled fine-grained sandstones for U-Pb detrital zircon analysis. We sought fresh, unexposed samples, and we removed weathering rinds with a rock hammer or shovel. Sampling localities, rock types, and other details are given in Table S1 and the locations are shown in Fig. 4. We blew dust off sampled rocks in the field and then again using compressed air in the laboratory in order to reduce the potential for contamination. Rock crushing, mineral separation, mount-making, geochronological analysis, and data reduction techniques closely followed those outlined by Dumitru et al. (2016) in their Data Repository.

We crushed rock samples and made zircon separates at Stanford University using standard procedures that included fracturing with a steel hammer followed by dust removal with compressed air, rock crushing, rock grinding, and concentration of denser grains using a modified Gemeni Table water-aided shaking apparatus. For the first of two sets of samples (15JLS002, 15JLS004, 15JLS015, 15JLS017, 15JLS027A, 15JLS029, 15JLS036B, and 15JLS037), which were separated in 2016, we employed a Frantz magnetic separator with 10º side slope and final (maximum) power setting of 2.3A to progressively remove magnetic grains. Dumitru et al. (2016) recommended a final power setting of 1.2A, so our higher setting may have removed some zircon grains containing inclusions or mantled by volcanic material, which could have resulted in lower yields of younger, primary volcanic grains (Naeser and Naeser, 1984) when these samples were analyzed at the University of California Santa Cruz. If this occurred, it would not weaken the integrity of maximum depositional ages (MDAs), but it could produce older MDAs for some samples, rendering the age constraints more conservative. Hence, for three samples initially separated in this manner in which we observed zircon in the magnetic fractions (15JLS029, 15JLS036B, and 15JLS037), we later (2018) combined all nonmagnetic fractions that were yielded from power settings of 1.2A and greater and extracted zircons again from these samples. These additional zircon separates, together with one additional sample not previously separated (15JLS041), were analyzed at the University of Arizona LaserChron Center.

Nonmagnetic mineral separates were fractionated by density using 3.32 g/cm^3 methylene iodide according to methods outlined by Dumitru and Stockli (1998). The resulting heavy fraction containing zircon was rinsed multiple times using deionized water. Zircon crystals were placed on an epoxy mount, photographed with the aid of an optical microscope, and then

analyzed. For the first group of samples, separated in 2016, analyses were conducted on an Element XR high-resolution magnetic-sector inductively coupled plasma mass spectrometer (ICP–MS) outfitted with a single collector and housed at the University of California, Santa Cruz, Institute of Marine Sciences. A total of 1000 analyses were conducted on sample grains. Our analyses were conducted using the 2015 instrument configuration and workflow described by Dumitru et al. (2016), but we selected slightly different parameters for laser ablation:

- Laser fluence: 4.0 J/cm^2
- Repetition rate: 8/s
- Shot count: 160 (20 s total duration)
- Spot size: 20 μm.

For these analyses, we employed Temora 2 zircon (416.78 ± 0.33 Ma isotope dilution–thermal ionization mass spectrometry weighted mean age by Black et al., 2004) as the primary age reference material (standard). A total of 210 grains of Temora 2 were analyzed, one after every fifth unknown age analysis, with additional Temora 2 analyses at the start and end of the session. We employed FC-5Z zircon (1099 ± 0.6 Ma; see Paces and Miller, 1993) as a secondary age reference material. One hundred eight analyses were made of FC-5Z. Mount Dromedary ("DROM") zircon (98.8 ± 0.6 Ma; White and Ireland, 2012) was employed as a tertiary age reference material and analyzed 50 times during the session. The zircon concentration reference material MADDER was used to estimate U, Th, and Pb abundances. MADDER was analyzed several times at the start of the session, and then once per approximately 50 other analyses.

Data reduction was conducted with the Iolite v.2.5 add-in to IGOR Pro v.6.3 (Paton et al., 2011) using the "U_Pb_Geochronology3" data reduction scheme. Baseline subtraction was applied using the "StepForward" spline. Baseline integrations were trimmed manually to exclude zones where ^{202}Hg and ^{204}Pb signal diverged from the mean of the baseline by 3 standard deviations or more. A correction for downhole fractionation was applied using Temora 2 as the reference material. Integration windows for the all reference materials were trimmed at the start and end in order to maximize the quality of fit of a double exponential downhole correction curve. We removed spikes of ^{204}Pb detected in Temora 2 analyses by manually trimming individual integrations away from the end. Finally, we interpolated signal between Temora 2 primary reference materials using "Spline_Smooth_Med5," which yielded the following statistics for final, downhole-corrected 206Pb/238U ages of the reference materials: MSWD =

0.92 for primary reference material Temora 2, MSWD = 1.1 for secondary reference material FC-5Z, and MSWD = 1.3 for tertiary reference material Mount Dromedary ("DROM"). Integrations of unknown analyses were deleted or trimmed away from the end according to criteria established by Dumitru et al. (2016). We employ their comment codes in our Table S2 as explanation for modifications to integration windows. We also add the comment "moved" in cases where the integration window was simply shifted due to a mismatch with the signal time series.

The single-collector ICP–MS at the UCSC Marine Sciences is unable to resolve ^{204}Pb due to isobaric interferences with ^{204}Hg, preventing the use of a ^{204}Pb-based common Pb correction. Instead, we applied a ^{207}Pb-based correction to ^{206}Pb/^{238}U ages ≤ 800 Ma using Isoplot v.3.75 (Ludwig, 2008). Although the 207-correction can yield erroneously young ages in cases where crystals have experienced significant Pb loss (Andersen et al., 2019), this correction is viable for younger grains (those ≤ ~800 Ma), and especially for those younger than ~100 Ma. This is because the common Pb composition is estimated by subtracting the radiogenic ^{207}Pb from the total. Since ^{238}U is much (137×) more abundant than ^{235}U, ^{206}Pb (from ^{238}U) is highly radiogenic, unlike ^{207}Pb (from^{235}U). Hence, at relatively young ages, subtracting out the radiogenic ^{207}Pb is more reliable because it represents a low proportion and will therefore result in a smaller potential correction. Because the youngest coherent group of ages for our samples (used to determine MDAs) is exclusively less than ca. 31 Ma, this method is especially viable for our study. Moreover, we applied a number of criteria, described below, to limit the potential that the correction could yield erroneously young ages.

In cases where the ^{206}Pb/^{238}U age exceeded 1000 Ma, we took uncorrected ^{207}Pb/^{206}Pb ages to represent the best age. We applied the following filtering criteria to omit analyses that exhibited discordance, reverse discordance, or potentially high common Pb:

- ^{206}Pb/^{238}U ages > 800 Ma and discordance > 30% relative to ^{207}Pb/^{206}Pb ages
- ^{206}Pb/^{238}U ages > 800 Ma and discordance < –7% (reverse discordance) relative to ^{207}Pb/^{206}Pb ages
- ^{206}Pb/^{238}U ages < 1000 Ma and ^{207}Pb-based common Pb correction to the ^{206}Pb/^{238}U ages > 10% relative to uncorrected ^{206}Pb/^{238}U ages
- ^{206}Pb/^{238}U ages ≥ 1000 Ma and ^{206}Pb/^{204}Pb < 250
- Extremely high errors (2σ) that are greater than the corresponding "best age."

There is no indication of systematic Pb loss among the grains to which the 207-correction were applied. The 207-correction was usually exceedingly small, as is documented in Table S2; the vast majority of grains were corrected by << 1 Ma (≤ 1%).

For the second group of samples, separated in 2018, analyses were conducted on a Nu Plasma multi-collector LA–ICP–MS attached to a Photon Machines Analyte G2 excimer laser at the University of Arizona LaserChron Center. Reference materials were supplied by the LaserChron Center and included their Sri Lanka (SL) zircon as a primary reference material and R33 (419.26 ± 0.39 Ma; Black et al., 2004) as a secondary reference material. Analytical procedures are outlined by Gehrels et al. (2006, 2008), and they include an automatic ^{204}Pb-based common Pb correction. The same filtering criteria were applied to this second group of samples. However, because the Nu Plasma multi-collector instrument is able to resolve ^{204}Pb, we also omitted analyses with ^{204}Pb > 700 cps.

Plots of weighted mean depositional or maximum depositional ages (Fig. S2) and age probability distributions (Fig. S1) were generated using Isoplot v.3.75. U-Pb ages by analysis and isotopic data used to calculate these ages are presented in Table S2. All weighted mean errors except for that of sample 15JLS029 are calculated according to the 95% confidence error of the weighted average. In the case of 15JLS029, only two grains are present in the youngest coherent group of ages, so we estimate the weighted mean errors using only the 2σ internal error (error propagated from only the assigned data-point errors), not multiplied by the square root of the mean square weighted deviation, MSWD). Only the young (≤ 70 Ma) analyses are shown in Fig. S2. Preferred MDAs (indicated in green) are typically based on the weighted mean of the youngest coherent group of analyses. Fig. S2 also presents weighted mean ages (indicated in black) with sufficient additional grains included to achieve MSWD ~1, although these are not our preferred ages.

Text S3. Procedures for Establishing Stratigraphic Thickness and Depositional Age Constraints

This section provides detailed information regarding how stratigraphic thicknesses were determined and how age constraints were applied throughout the stratigraphic sections presented

in Figs. 5 and 6. Sample localities are shown in Figs. 3 and 4 and listed in the Supplementary Data Tables.

Pliocene–Pleistocene Hay Ranch Formation

Depositional ages are not well constrained for the Hay Ranch Formation, which is the youngest unit considered in this study. The stable isotope results for this unit that are shown in Fig. 5 were originally obtained by Horton et al. (2004), who did not report sample locations but assigned ages based on assumed sedimentation rates. We assume that these samples were collected from Pine Valley, west of the Piñon Range, in the general location indicated in Fig. 3. Regnier (1960) and Smith et al. (1976) provided a tentative depositional age range for the Hay Ranch Formation of middle Pliocene to middle Pleistocene. We therefore assume a permissible depositional age range of 3.6–1.8 Ma for Horton et al.'s samples. Lacking information about stratigraphic depths, for visualization purposes in Fig. 6 we plot all samples as being deposited at the same time, and we retain the full permissible depositional age ranges in the error bars.

Oligocene–Miocene Humboldt Formation

The latest Oligocene to Miocene Humboldt Formation (Sharp, 1939) is described in detail by Wallace et al. (2008), Lund Snee (2013), Lund Snee and Miller (2015) and Lund Snee et al. (2016). Lund Snee et al. (2016) observed a clear pattern of upward-younging ages for tuffs sampled within the Humboldt Formation. For the present study, we collected additional samples for geochronology and stable isotope analysis in several measured sections shown in Fig. 5, which add to the geochronologic data presented by Lund Snee et al. (2016). The lowest exposed levels of the Humboldt Formation were sampled in two subparallel sections near the westernmost exposures of the Humboldt Formation in the studied area, as well as a third "eastern base Humboldt Formation" section northeast of Cedar Ridge (shown in Figs. 3 and 4), for redundancy across this important interval. Samples are described from older to younger in each of these sections.

Using map relationships, stratigraphic thicknesses and depositional age constraints, the two western sections were compiled together in the "composite western base Humboldt Formation" section (Figs. 4b and 5). In our thickness measurements for this compiled section, we accounted for minor observed offset and duplication of Humboldt Formation strata across an E-

striking fault in the northern of the two sections (~48 m stratigraphic thickness duplicated). An absolute maximum age constraint for this section (and for the Humboldt Formation across the area) is 31.08 ± 0.47 Ma ($^{40}Ar/^{39}Ar$ sanidine), our preferred age obtained for the tuff of Hackwood Ranch, which the Humboldt Formation overlies across a poorly exposed angular unconformity (Lund Snee et al., 2016). Above this, only a few meters above the base of this unit in the composite western section, we obtained a U-Pb detrital zircon MDA of 25.1 ± 0.2 Ma (Fig. S2b) from a sample of air-fall tuff deposited within the Humboldt Formation (sample 15JLS002; Fig. 4b). Lund Snee et al. (2016) obtained a U-Pb detrital zircon MDA of 24.4 ± 0.1 Ma from their sample ELM11-PN19, collected from about 60 m stratigraphically above 15JLS002, also from a probable air-fall tuff deposited within the Humboldt Formation, which provides another approximate absolute depositional age for that low stratigraphic level (Fig. 5). Together, these progressively younger ages within the Humboldt Formation reveal minor but sustained lacustrine deposition well before major surface-breaking extension initiated ca. 17–16 Ma (Colgan and Henry, 2009; Colgan et al., 2010; Lund Snee et al., 2016).

The lowest Humboldt Formation samples that yielded stable isotope values in this western composite basal section (samples 15JLS003A and 15JLS028) lie between the sample dated as 24.4 Ma and overlying sample 15JLS004 which yielded an MDA of 21.7 ± 0.1 Ma based on a weighted mean of 75 grains (Fig. S2c). These two intervening samples were assigned ages of 24 and 23 Ma, respectively, based on their relative position in the section (assuming constant depositional rates). A single grain in sample 15JLS004 that displayed obvious zoning was omitted, but the earlier part of this grain's analytical time series yielded a young age of 15.7 ± 0.9 Ma. Hence, we note that it is possible that sample 15JLS004 (and those above it) may be ca. 15.7 Ma or younger, but the tenuous nature of this zoned single grain age and the sample's stratigraphic position (near and below samples containing only older ages) makes that possibility less likely. Although the large population of grains ca. 22 Ma (Fig. S2c) in this sample (n = 91) suggests that it may represent a reworked air-fall tuff, we conservatively do not treat this sample as a bound on minimum depositional ages for underlying strata due to the uncertainty related to the possible younger grain. Sample 15JLS027A, from ~11 m below 15JLS028, was not helpful for establishing section ages as it yielded a poorly constrained MDA of 25.3 ± 1.2 Ma based on a single zircon grain (older than age constraints beneath it). Sample 15JLS005 (from the southern section) was assigned an MDA of 19.0 Ma. Stratigraphically overlying sample 15JLS029 (from

the northern section) yielded an MDA of 18.4 ± 2.5 Ma, based on a weighted mean of 3 ages (Fig. S2f). A weighted mean age of 16.6 ± 0.3 (Fig. S2d), from 8 grains, is established for a higher sample from the southern section, 15JLS017. This sample provides an MDA for several stratigraphically overlying stable isotope analyses obtained in this study (15JLS018, 15JLS021, 15JLS022, 15JLS030A, 15JLS030B) as well as from previous work by Mulch et al. (2015) and sources therein. A minimum depositional age of 15.53 Ma is assigned to the same samples (and to stratigraphically underlying samples), based on a U-Pb detrital zircon age of 15.6 ± 0.1 Ma obtained by Lund Snee et al. (2016) for air-fall tuff sample Tiws-J4 (Fig. 5). Higher in this composite section, approximate absolute depositional ages reported by Lund Snee et al. (2016) on upward-younging, intercalated air-fall tuffs provide maximum and minimum depositional age constraints on overlying and underlying strata, respectively (Fig. 5). These ages enable us to assign depositional age bounds on the stable isotope samples reported by Mulch et al. (2015) and sources therein for the upper (northern) portions of their "Indian Well Formation" section (see Figs. 3, 4b, and 5). (Note that Lund Snee et al., 2016, recommended that the Indian Well Formation nomenclature be discontinued after they found that essentially all sedimentary strata previously included within it are latest Oligocene to Miocene in age and belong to the Humboldt Formation based on detailed re-mapping of the section by Lund Snee and Miller, 2015).

The eastern section, which also contains the base of the Humboldt Formation, is exposed ~8 km away from the western section described above, on the northeast side of Cedar Ridge (Figs. 3 and 4c), across a normal fault system that duplicates the Cenozoic succession (Wallace et al., 2008; Lund Snee and Miller, 2015; Lund Snee et al., 2016). In the eastern section, strata of the Humboldt Formation were deposited unconformably above rocks resembling the Eocene Elko Formation and Late Cretaceous(?)–Eocene(?) limestone (TKl) and conglomerate, sandstone, siltstone, and limestone (TKcs) units (Lund Snee and Miller, 2015; Lund Snee et al., 2016). Unlike the composite basal section exposed further west, detrital U-Pb zircon analyses carried out in this succession (sample 12HBD06 of Lund Snee et al., 2016, and sample 15JLS036B of this study) record no grains in the age range between the end of local volcanic activity at ca. 37 Ma and the onset of rapid extension ca. 17–16 Ma (Colgan et al., 2010; Lund Snee et al., 2016). The lowest sample collected near the base of the Humboldt Formation (sample 12HBD06 of Lund Snee et al., 2016) contained a single young grain at 15.7 ± 0.5 Ma, which provides a tentative MDA. The lack of grains older than 15.7 Ma suggests that sedimentation did

not occur in this eastern area in the time span ~26–15.7 Ma, when tuffs were being deposited in the Humboldt Formation succession sampled ~8 km to the west. Nevertheless, because of the lack of better age constraints at the base of the eastern section below sample 12HBD06, we very conservatively plot error bars for the three lowest stable isotope samples (15JLS031A, 15JLS031B, and 15JLS033) to possibly extend to as old 24.4 Ma, the absolute depositional age of sample ELM11-PN19 (Lund Snee et al., 2016) from near the bottom of the western section (Fig. 4). Most likely, however, the stable isotope samples are close in age to the (tentative) ca. 15.7 Ma MDA obtained from overlying sample 12HBD06, so they are plotted in Fig. 5 with depositional ages between 16.5–16.0 Ma.

An MDA of 12.0 Ma is tentatively given to the uppermost part of this eastern basal Humboldt Formation succession (Figs. 3 and 4c) on the basis of a single U-Pb zircon age of 11.5 ± 0.4 Ma obtained in sample 15JLS036B (Fig. S2g). Although minimum depositional ages are not constrained for this eastern succession, the stratigraphic position of these samples and the observation of numerous intercalated tuffs within the succession suggests that they were unlikely to be deposited much later than 11.1 Ma (the MDA of the same sample 15JLS036B accounting for the young grain's 2σ uncertainty). It is especially unlikely that samples from this eastern section were deposited after 9.91 Ma, which is the youngest depositional age obtained by Wallace et al. (2008) using isotopic dating methods and tephra correlations on tuffs collected further up-section, east of Huntington Creek (Fig. 4d).

Finally, we sampled a fourth Humboldt Formation section to the northeast of the others, near the Lee township (Fig. 3), part of which Chamberlain et al. (2012) and Mulch et al. (2015) previously sampled for stable isotope values but did not have age constraints. We have bracketed the MDA for this succession with a U-Pb detrital zircon age of 14.9 ± 0.2 Ma obtained on tuff sample 15JLS041, from the base of the section (Figs. S2i, 4d, and 5). We account for local duplication by open folds shown in Fig. 4d, as well as minor, outcrop-scale normal faults. At the top of the section, we obtained a U-Pb detrital zircon age of 12.4 ± 1.0 Ma, on sample 15JLS037 (Fig. S2h), which establishes an MDA for stable isotope analyses obtained on that same sample. Although this MDA does not provide an upper (minimum) age constraint, the section is approximately along strike from (and ~5 km away from) the Humboldt Formation type section on the eastern banks of Huntington Creek (Sharp, 1939) in which Wallace et al. (2008) found air-fall tuff depositional ages ranging from 15.31 Ma at the base to 9.91 Ma at the top (Fig. 3). The

youngest detrital zircon MDA obtained for the Humboldt Formation in Huntington Valley is 8.2 ± 0.2 Ma (Lund Snee et al., 2016, sample 12HBD09), from a sample collected ~10 km southwest of the Lee section sampled in this study. We assign best ages to the Lee section that range between 14.87–11.80 Ma considering the above information and assuming constant sedimentation rates, but we allow the uncertainty bars plotted in Fig. 6 to span as young as 8.01 Ma.

Eocene–Oligocene sandstone and siltstone between the Eocene tuff of Dixie Creek and the Oligocene tuff of Hackwood Ranch

A thin (< 200 m) deposit of sandstone and siltstone is exposed near the abandoned Hackwood Ranch site (Figs. 3 and 4a). The depositional ages for these strata are bracketed by a 36.84 ± 0.34 Ma (U-Pb zircon SHRIMP) age for the unconformably underlying tuff of Dixie Creek and multiple 31.10 Ma ($^{40}Ar/^{39}Ar$ sanidine and U-Pb zircon SHRIMP) eruptive ages for the overlying tuff of Hackwood Ranch (Lund Snee et al., 2016). Hence, deposition of this sedimentary succession occurred across the time interval 37.18 to ca. 31 Ma. In addition, Lund Snee et al. (2016) reported a U-Pb detrital zircon MDA of 33.9 ± 0.4 Ma for a sample (10JLS08) collected from the lower parts of this interval, and we (this study) obtained a U-Pb detrital zircon MDA of 29.9 ± 0.2 Ma for a sample (15JLS015) collected from near the top of the succession, based on a weighted mean of 45 grains (Figs. 4a, 5, and S2a). Two grains were omitted due to the indication of zoning in their time series. It is unclear why this upper MDA is ≥ 0.5 Ma younger than (outside of the uncertainty range of) the age of the overlying tuff of Hackwood Ranch. We consider the previously reported ages for the tuff of Hackwood Ranch to be definitive due to the consistency of these ages across multiple isotopic systems (Lund Snee et al., 2016), and the expectation that single collector LA–ICP–MS analysis could be less accurate than U-Pb SHRIMP or $^{40}Ar/^{39}Ar$. Samples collected from this section for the present study did not contain sufficient carbonate material for stable isotope analysis, but these rocks are reported here because they nevertheless document localized sediment accumulation during that time span.

Eocene Elko Formation

Numerous detrital (maximum depositional) and tuff (depositional) ages have been obtained by previous workers from Eocene Elko Formation samples. Across the Elko Basin, the

beginning of Elko Formation deposition is approximately bracketed by a pink air-fall tuff at low stratigraphic levels in the Elko Hills (Fig. S3) that yielded a U-Pb zircon (SHRIMP) age of 46.1 ± 0.2 (sample 00-188GS of Haynes, 2003), which is probably correlative with a less precise U-Pb detrital zircon age of 45.92 ± 0.95 Ma obtained by Lund Snee et al. (2016) further south (sample ELKO-1). Here we take the more precise 46.10 ± 0.20 Ma age obtained by Haynes (2003) to conservatively suggest an approximate start of Elko Formation deposition at 46.30 Ma (including the 2σ uncertainty). An eruptive age of 38.47 ± 0.15 Ma ($^{40}Ar/^{39}Ar$ plagioclase) obtained from a basal eruptive unit within the overlying tuff of Dixie Creek (sample H10-45 of Henry et al., 2015) provides a minimum depositional age of 38.32 Ma for the Elko Formation. A U-Pb detrital zircon weighted mean age of 37.9 ± 0.5 Ma from the eastern Piñon Range (sample ELKO-2 of Lund Snee et al., 2016) indicates that deposition of the Elko Formation continued at least to that time, bracketing the youngest Elko Formation deposition to around ca. 38.4 Ma (accounting for 2σ uncertainties). The ages of the uppermost Elko Formation strata and the lowermost overlying tuffs suggest that Elko Formation deposition continued until the onset of volcanism in this area.

None of these bracketing ages were obtained from samples collected within the immediate area of the Elko Formation section studied for stable isotope values by Horton et al. (2004) and subsequent studies (Mix et al., 2011; Chamberlain et al., 2012; Mulch et al., 2015), which is located near Emigrant Spring (Fig. 3). However, Mulch et al. (2015) obtained $^{40}Ar/^{39}Ar$ ages from detrital biotite collected across this same section, which permit establishment of MDAs throughout the sampled section. With one exception, these MDAs young upward, which could indicate that some of them represent air- or water-lain tuffs that originated from nearby eruptions of similar ages (Ressel and Henry, 2006). Accounting for this possibility, in Fig. 6 we select a best estimate of actual depositional age for each sample according to the possibility that some of the ages provided by Mulch et al. (2015) could represent absolute depositional ages, but we conservatively plot error bars that extend upward to the true minimum depositional age bound of 38.32 Ma provided by tuff sample H10-45 of Henry et al. (2015).

Horton et al. (2004) assigned additional samples at the base of this section to underlying "Cherty Limestone" and "Limestone and Limestone clast Conglomerate" units (the same samples were assigned to units called "Cherty Limestone" and "Limestone and Conglomerate" by Mulch et al., 2015). Mulch et al. (2015) reported that these samples were collected from a

section near Emigrant Spring (Fig. 4). However, Horton et al. (2004) did not report sample locations, so the exact stratigraphic assignment and age cannot be determined. Horton et al. (2004, p. 864) identified these rocks as belonging to the "non-volcanic sequence" of early Cenozoic strata that precedes the Elko Formation, which would make them older than ca. 46 Ma, although Mulch et al. (2015) placed the 46.1 Ma tuff age obtained by Haynes (2003) between the "Cherty Limestone" and "Limestone and Conglomerate" units, based on stratigraphic assignments made further north in the Elko Hills, implying that the overlying "Cherty Limestone" is younger than 46.1 Ma and the "Limestone and Conglomerate" is older.

This confusion may be at least partly resolved by the recent observation of Cenozoic volcanic clasts in a basal conglomerate within the Elko Formation from which a U-Pb zircon MDA of 44.5 ± 0.9 Ma was also obtained (sample EmigZr7 of Hollingsworth et al., 2017). This sample was collected from 50–85 m above the unconformity with underlying Paleozoic rocks at the Emigrant mine location (Ressel et al., 2015), which is ~3.5 km north of the Emigrant Spring section studied by Horton et al. (2004) and Mulch et al. (2015) and included in this study (Figs. 5 and 6). For this reason, the strata that were previously assigned by Horton et al. (2004) and Mulch et al. (2015) to underlying units called "Cherty Limestone" and "Limestone and Conglomerate" (and similar) most likely belong to the lower part of the Elko Formation and are probably for the most part 45.4 Ma and younger, counting the 2σ age uncertainty (Figs. 5 and 6). Because that age was not obtained from a sample from the absolute bottom of the Elko Formation, we conservatively assign these basal Elko Formation strata an older MDA constraint of 46.3 Ma, the oldest age obtained from the Elko Formation (2σ uncertainty range of sample 00-188GS of Haynes, 2003). Based on these age constraints, we assign a *preferred* depositional age of 45.0 Ma to the stratigraphically lowest "Limestone and Conglomerate" sample in Fig. 5 (TL04-02). Because locations and stratigraphic depth information are not available for this unit and the "Cherty Limestone" of Horton et al. (2004) and Mulch et al. (2015), we assign best ages that decrease upward in increments of 0.1 Ma (to 44.3 Ma). As with some of the overlying strata of the middle Elko Formation described above, we employ a minimum depositional age bound of 41.2 Ma for these units, based on the 2σ range for the 41.60 ± 0.40 Ma reworked sediments analyzed by Mulch et al. (2015).

Finally, we note that Smith et al. (2017) challenged the use of $^{40}Ar/^{39}Ar$ biotite ages for obtaining precise ages, and they argued that the biotite ages reported by Mulch et al. (2015) were

erroneously young. Smith et al. (2017) presented single-crystal $^{40}Ar/^{39}Ar$ sanidine ages from ash beds that yielded ages ca. 1.5–2.0 Myr older than those represented by the biotite. Partly on this basis, they argued that Elko Formation deposition ceased by ca. 40.4 Ma. However, as described above, multiple mineral and isotopic systems indicate that Elko Formation deposition continued nearby until ca. 38.4 Ma, which is clearly at odds with those significantly older estimates. In addition, sanidine from the same Elko Formation strata sampled by Mulch et al. (2015) yielded $^{40}Ar/^{39}Ar$ ages that are slightly *younger* than their reported biotite ages by 0.3–0.8 Ma, and indistinguishable within 2σ error (M. Cosca, 2019, pers. comm.). It is therefore puzzling that Smith et al. (2017) obtained systematically older ages on some of the same strata. We suggest that the discrepancy could have occurred if the $^{40}Ar/^{39}Ar$ sanidine ages reported by Smith et al. (2017) included older detrital sanidine populations. This could be a possibility given that numerous closely-spaced Cenozoic age populations have been observed in Elko Formation samples (Lund Snee et al., 2016), and that appreciable fluvial and lacustrine reworking of air-fall tuffs occurred during deposition (Haynes, 2003).

Late Cretaceous(?)–early Eocene(?) limestone (TKl) and conglomerate, sandstone, siltstone, and limestone (TKcs)

Late Cretaceous(?)–early Eocene(?) limestone (TKl) and conglomerate, sandstone, siltstone, and limestone (TKcs) units underlie the Elko Formation near Cedar Ridge (Figs. 3 and 4) and are apparently older than the oldest strata sampled for this study (Fig. 5). Hence, these units are likely older than 46.10 ± 0.20 Ma, which is the age of the oldest volcanic tuff observed at the base of the Elko Formation (sample 00-188GS of Haynes, 2003). The MDA of these underlying sediments is constrained only by the presence of fossils "younger than Jurassic" (I.G. Sohn in Smith et al., 1976), with the bulk of fossil evidence provided by Smith et al. (1976) pointing to deposition occurring in Late Cretaceous time or later, and a youngest detrital zircon population of 240 Ma (sample ELM11-PN16 of Lund Snee et al., 2016). Based on this information, we assume that the likeliest age for units TKcs and TKl is Late Cretaceous–Eocene (100 Ma to 45.9 Ma, counting the 2σ error for sample 00-188GS). The limestone unit (TKl) is thought to be slightly younger than the clastic unit (TKcs) on the basis of its generally higher stratigraphic position, although they could be partially contemporaneous (Lund Snee et al., 2016). We note that Ketner and Alpha (1992) argued that the "cherty limestone" and

“conglomerate” facies in the Emigrant Spring area and elsewhere should be included within the Eocene Elko Formation due to apparently conformable relations with the overlying Elko Formation rocks and because similar cherty limestone and conglomerate rocks are clearly part of the lower Elko Formation further north in the Elko Hills (Fig. 3). Despite this, we consider the conspicuous lack of Cenozoic volcanic detritus in these older rocks within the study area to be diagnostic and to potentially provide important information about stratigraphic age. Hence, we follow Smith et al. (1976), Lund Snee (2013), and Lund Snee and Miller (2015) and separate the TKcs and TKl units from the younger Elko Formation where these sediments demonstrably lack Cenozoic detritus.

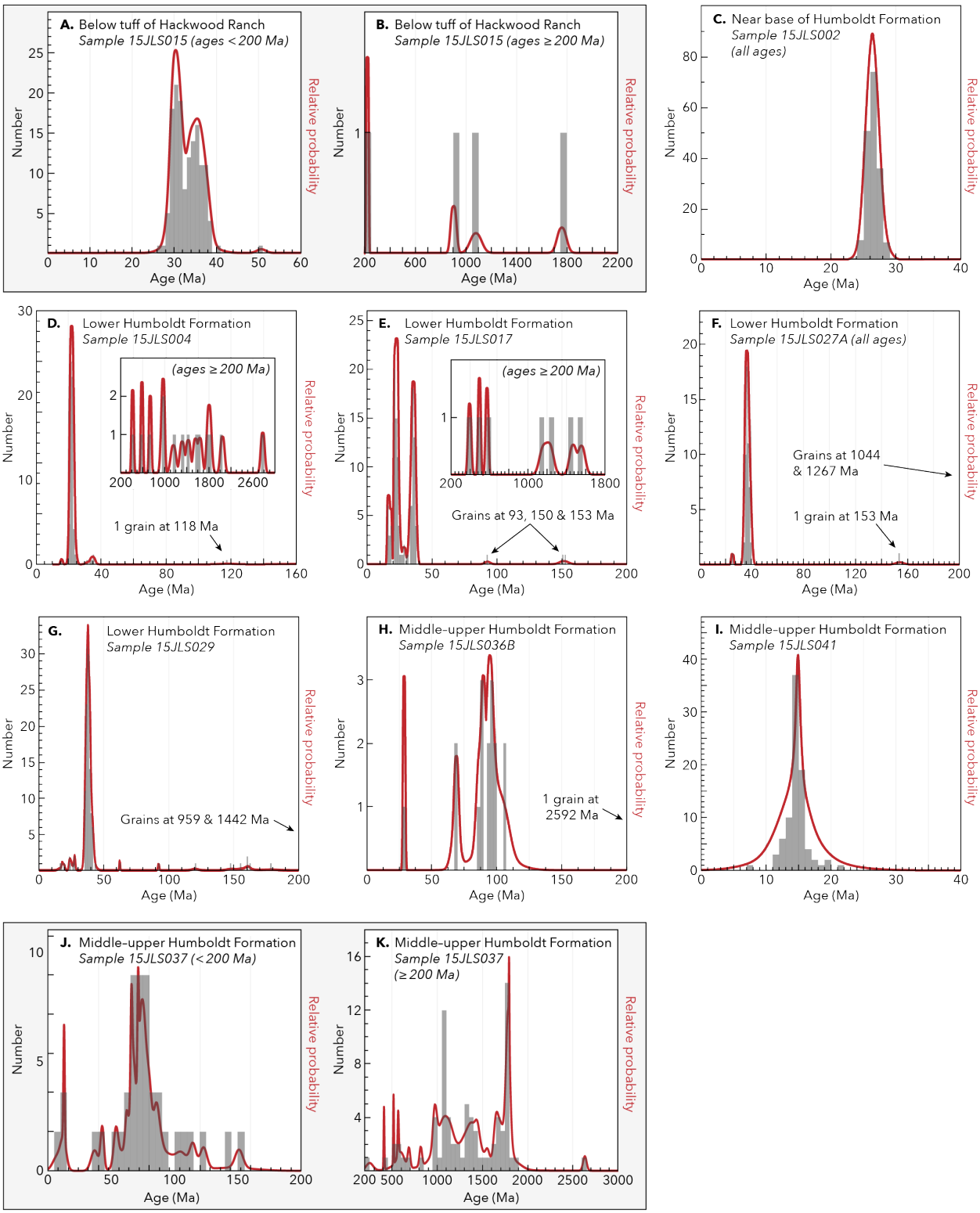

Fig. S1. Probability density plots of detrital zircon U-Pb ages.

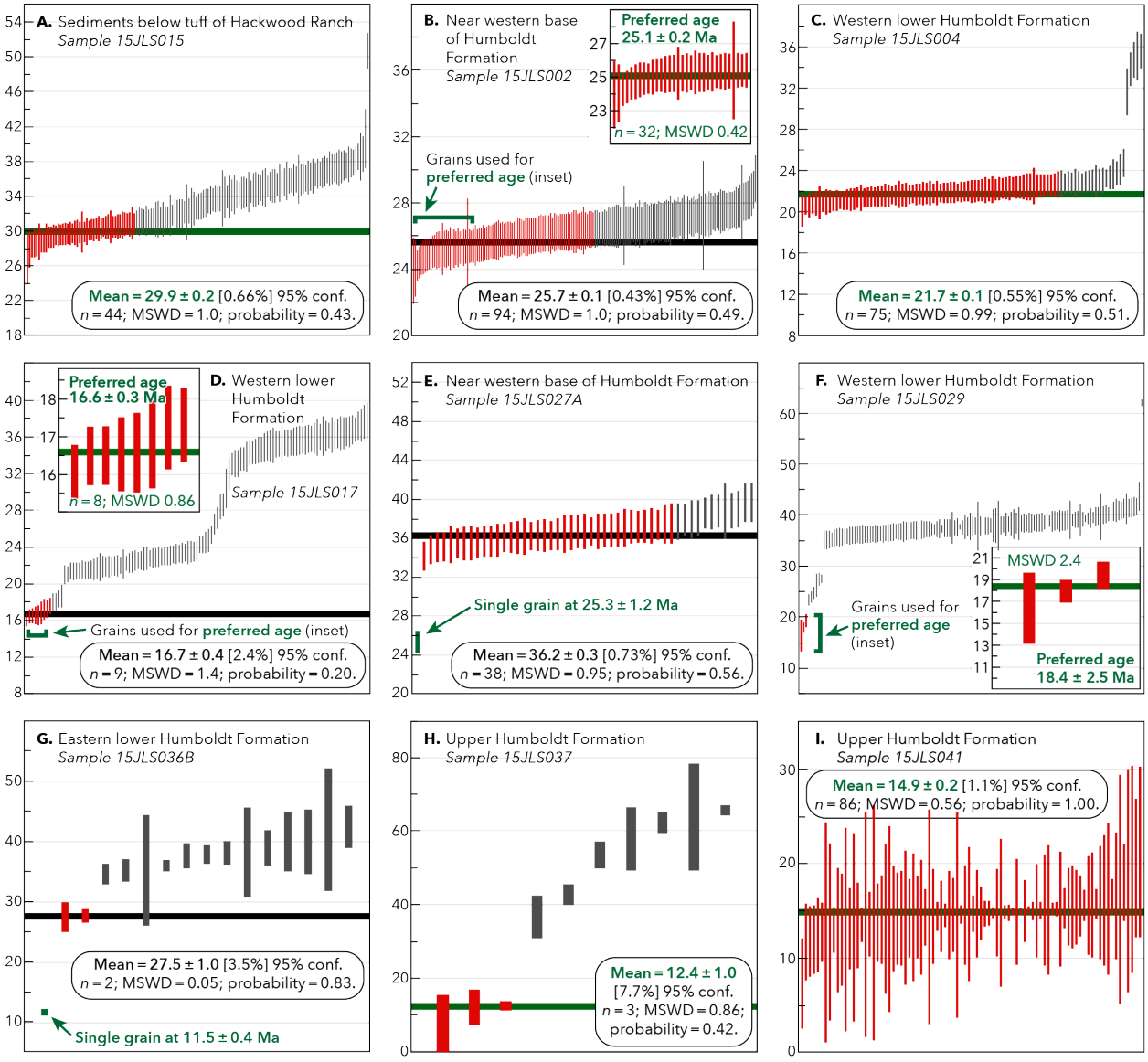

Fig. S2. Weighted mean plots for the youngest coherent groups of detrital zircon U-Pb analyses obtained from each sample, defining depositional ages or maximum depositional ages. Preferred ages are indicated in green and are also given in Table S1. Non-preferred weighted mean ages (black) are given to indicate the youngest group of ages yielding MSWD ~1. Weighted by data-point errors only. Box heights represent 2σ errors. MSWD = mean square weighted deviation.

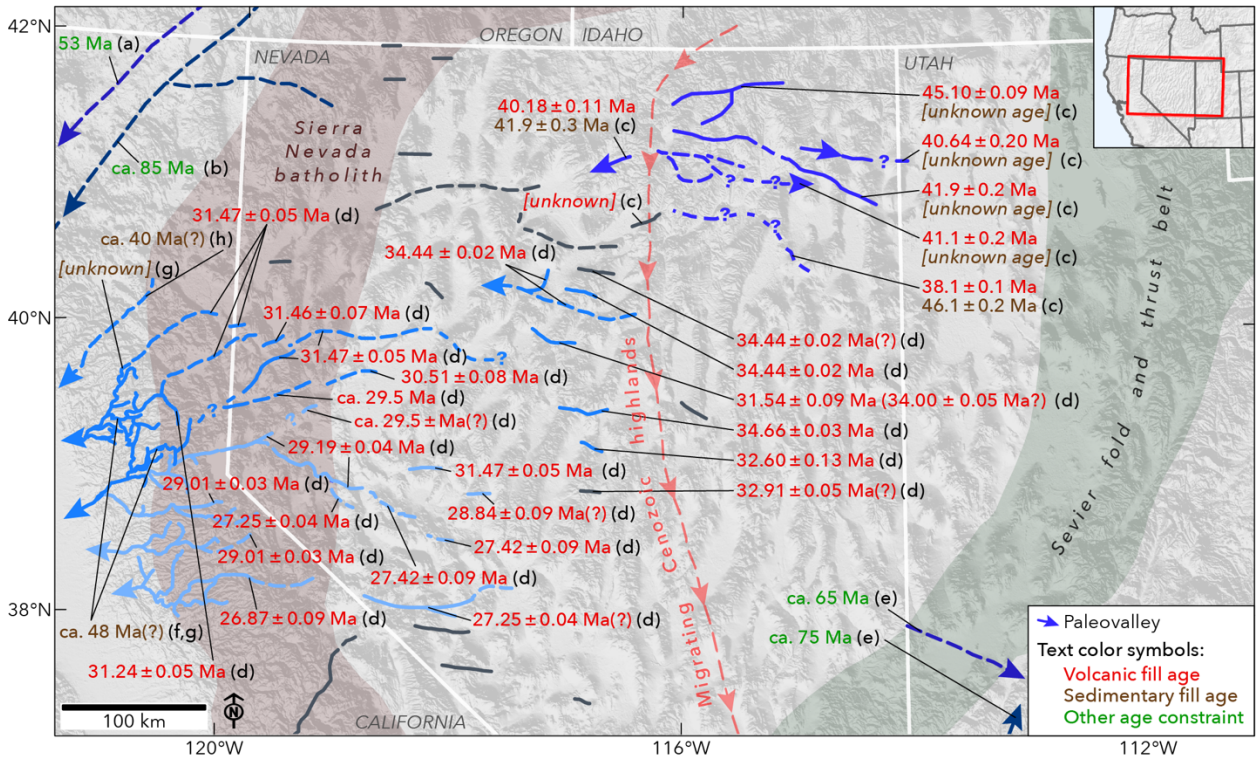

Fig. S3. Map of paleovalleys from the Great Basin and surroundings, western USA, with data sources and ages of oldest fill material or onset of drainage activity indicated. Paleovalley locations are from Henry et al. (2012), Henry and John (2013), Dumitru et al. (2015, 2016), and sources therein. Oldest sedimentary and/or volcanic fill identified in each paleovalley are indicated (orange and red type, respectively). Ages of pre-volcanic sedimentary fill are not well constrained. Grey paleovalleys indicate no relevant age constraints. The Sevier fold and thrust belt is from DeCelles (2004). The Cretaceous Sierra Nevada arc is after Van Buer and Miller (2010). This figure complements Fig. 2, providing additional age information and references. (a)—Dumitru et al. (2015); (b)—Dumitru et al. (2016); (c)—Henry (2008); (d)— Henry and John (2013); (e)—Goldstrand (1992, 1994); (f)—MacGinitie (1941); (g)—Yeend (1974); (h)—Garside et al. (2005).